Xuan Liu
The Combustion Laboratory,
Department of Mechanical Engineering,
University of Maryland,
College Park, MD 20742;
State Key Laboratory of Multiphase Flow in Power Engineering,
School of Energy and Power Engineering,
Xi'an Jiaotong University,
Xi'an 710049, China
e-mail: liuxuanne@foxmail.com

Kiran Raj G. Burra
The Combustion Laboratory,
Department of Mechanical Engineering,
University of Maryland,
College Park, MD 20742
e-mail: kiranraj@umd.edu

Zhiwei Wang
The Combustion Laboratory,
Department of Mechanical Engineering,
University of Maryland,
College Park, MD 20742;
College of Environmental Engineering,
Henan University of Technology,
Zhengzhou 450001, China
e-mail: bioenergy@163.com

Jinhu Li
The Combustion Laboratory,
Department of Mechanical Engineering,
University of Maryland,
College Park, MD 20742;
School of Safety Engineering,
China University of Mining and Technology,
Xuzhou 221116, China
e-mail: ljh_cumt@163.com

Defu Che
State Key Laboratory of Multiphase Flow in Power Engineering,
School of Energy and Power Engineering,
Xi'an Jiaotong University,
Xi'an 710049, China
e-mail: dfche@mail.xjtu.edu.cn

Ashwani K. Gupta[1]
The Combustion Laboratory,
Department of Mechanical Engineering,
University of Maryland,
College Park, MD 20742
e-mail: akgupta@umd.edu

Syngas Characteristics From Catalytic Gasification of Polystyrene and Pinewood in CO_2 Atmosphere

Syngas production from catalytic gasification of polystyrene and pinewood in CO_2 atmosphere was investigated over Ni-Mg/Al_2O_3 catalyst in a fixed-bed reactor at 900 °C. A quasi in situ method was adopted for catalytic gasification wherein the catalyst placed downstream of the feedstock in the same reactor was used for enhanced syngas production. The effect of catalyst on evolutionary behavior, cumulative syngas yield, syngas composition, and cold gas efficiency was systematically analyzed. The results showed that addition of catalyst for polystyrene gasification resulted in enhanced yields of 63% H_2, 20% CO, 119% CH_4, and 85% C_2-C_3 yields. Enhanced H_2 and light hydrocarbon yields were mainly from enhanced cracking of pyrolytic vapors from polystyrene degradation, while the CO yield was attributed to CO_2-assisted reforming of benzene derivatives from primary cracking and polycyclic aromatic hydrocarbons (PAHs) from secondary gas phase condensations. The yields of H_2, CO, CH_4, and C_2-C_3 from pinewood gasification in the presence of catalyst was also enhanced by 150%, 14%, 39%, and 16%, respectively, indicating that Ni-Mg/Al_2O_3 catalyst can efficiently enhance syngas production in CO_2-assisted gasification. A comparison of syngas composition between non-catalytic and catalytic conditions revealed improved syngas quality in catalytic gasification with increased H_2 mole fraction but decreased CO mole fraction. Furthermore, cold gas efficiency enhanced from 44% to 57% in catalytic polystyrene gasification, and from 75% to 94% in catalytic pinewood gasification. The results suggest that catalytic CO_2 gasification offers a promising pathway for efficient energy production from wastes plastics and biomass while simultaneously using CO_2. [DOI: 10.1115/1.4049587]

Keywords: Ni-catalyst, CO_2 gasification, plastic wastes, syngas production, energy efficiency, alternative energy sources, energy conversion/systems, energy from biomass, hydrogen energy

1 Introduction

According to the United States Environmental Protection Agency (EPA), the generation of municipal solid waste (MSW) in the United States has increased sharply from 88.1 million tons in 1960 to 292.4 million tons in 2018 [1]. It is expected that waste generation will continue to increase due to enhanced lifestyle with growing consumption of energy and materials. The dramatical increase in waste generation with lack of sustainable disposal protocols poses a severe threat to the environment. This gives opportunities to the researchers to develop environmentally friendly energy-utilization methods for the hydrocarbons present in waste management. Plastic waste is a typical MSW that represented 12.2% share (35.7 million tons) in total MSW in the United States in 2018 [1]. The generation of plastic wastes has also increased due to increased use of different plastics for packing,

[1]Corresponding author.

Contributed by the Advanced Energy Systems Division of ASME for publication in the Journal of Energy Resources Technology. Manuscript received December 8, 2020; final manuscript received December 18, 2020; published online January 27, 2021. Editor: Hameed Metghalchi.

household goods, automotive parts, and industrial appliances [2]. However, recycling these post-consumed plastics is difficult not only due to the challenges associated with separating plastics from waste stream but also due to their varying recycled value for different plastics [3]. In 2018, only 8.5% of generated plastic wastes in the United States were recycled and over 70% of these plastic wastes were discharged to the environment or ended up in landfills [1]. Specifically, the recyclability of polystyrene (PS) was worse with a recycling rate of only around 0.8% [4]. It is estimated that approximately 20 million tons PS wastes are generated across the world per year [5]. These PS wastes are not biodegradable and can cause serious problems, especially to marine environments [6]. Most recently, researchers have reported that the discharged plastics can break down into small fragments (also referred as microplastics) in the presence of ultraviolet light [7]. These small-sized microplastics are considered as emerging contaminants and their potential hazards to the environment have not been fully understood [8]. Furthermore, plastics are petro-derived products and characterized with high-calorific values [9]. Discharging or landfilling these plastic wastes results in the loss of potential fossil fuel energy that can be converted to fuels and chemicals. In this context, it is desirable to develop innovative energy recovering processes based on waste plastics (especially PS wastes) to address issues on both waste management and energy needs.

In contrast, forestry and agricultural wastes are abundant lignocellulosic biomass that can be used as feedstocks for sustainable energy and fuel production. The global biomass production is estimated to be approximately 100 billion tons per year [10]. Biomass is an attractive carbon neutral resource that can help assist to counter global warming and air-quality deteriorating resulting from the rising CO_2, NOx, and SOx emissions from the utilization of conventional fossil fuels [11]. In addition, some low-grade biomass wastes, such as paper and cardboard, food wastes, and yard trimmings accounted for over half of the total MSW generation in the United States in 2018 [1]. The utilization of forestry and agricultural residues, as well as low-grade biowastes for energy production can foster energy sustainability and help reduce the land size requirements for landfilling these wastes.

Gasification is a thermochemical process that involves mild oxidation of solid carbonaceous material in the presence of some gasifying agent (such as steam, CO_2, O_2, or air) to produce high-calorific value syngas rich in H_2, CO, and light hydrocarbons [12]. The obtained syngas can be directly adopted for heat and power generation or further used as feedstock to synthesize value-added chemicals [13]. In recent years, gasification of plastic wastes and biowastes has received growing attention as this technology provides a promising pathway for simultaneous energy production and waste disposal. Basha et al. [14] performed air co-gasification of PS and palm kernel using an electrically heated downdraft gasifier at temperatures of 700–900 °C. They found that increase in gasification temperature resulted in higher H_2 and CO volume fractions but lower CH_4 volume fraction in the collected syngas and that an increase in PS content in the feedstock blend enhanced syngas production at 900 °C. Burra and Gupta [3] examined syngas characteristics from steam gasification of pinewood and different plastic wastes (polyethylene-terephthalate (PET), black polycarbonate (BPC), and polypropylene (PP)). Their results showed that co-gasification of biomass and plastic wastes led to non-additive enhancement of syngas yield, mainly from enhanced H_2 and CO yields during their co-gasification. Even though these studies successfully demonstrated the syngas production from gasification of plastic wastes and biomass, tar formation remains as one of the challenges in gasification that hinders commercialization of this technology. Tar is a by-product during pyrolytic breakdown of the feedstock material and is produced from a series of complex thermochemical reactions during gasification [15]. In addition, gasification of plastic wastes typically produced higher tar content than biomass gasification [16]. Utilization of raw syngas containing tar can cause corrosion and blockage of downstream equipment, and in turn decrease overall process efficiency [17]. To solve this problem, application of catalyst in gasification has received considerable attention as it can effectively reduce tar formation from enhanced tar reforming and cracking reactions [18,19]. Ruoppolo et al. [20] investigated catalytic steam gasification of biomass/plastic pellets (containing 80 wt% pinewood sawdust and 20 wt% polyethylene (PE) chips) using a fluidized bed gasifier. Ni/Al_2O_3 was used as an in-bed catalyst. Their results showed that the presence of steam reduced tar concentration and increased H_2 production, so that the presence of catalyst played a more pronounced role in tar reduction and H_2 enhancement. Alvarez et al. [21] reported catalytic steam gasification of biomass and plastics mixtures using a two-stage pyrolysis/gasification process, wherein the blended feedstocks were pyrolyzed in the first reactor and the pyrolytic vapors reformed in the second catalytic reactor in the presence of steam to maximize H_2 production. They found that the addition of catalyst remarkably improved the syngas yield and H_2 concentration, resulting from the catalytically enhanced steam reforming and water gas shift reactions. Kim et al. [22] studied air gasification of mixed plastic wastes using dolomite and activated carbon as catalysts in a two-stage gasifier. Activated carbon showed a better performance than dolomite for tar removal. When activated carbon was used as the catalyst, H_2 production was two times higher while tar production was 2.5 times lower than non-catalytic condition.

Despite these catalytic gasification studies performed in steam or air atmospheres, to the best of our knowledge, very limited information is available on catalytic gasification of plastic wastes and biomass in CO_2 atmosphere with a focus on syngas production and energy efficiency. Catalytic CO_2 gasification is expected to enhance tar cracking and dry reforming reactions, thereby improving process efficiency, and simultaneously converting CO_2 into fuel during disposal of waste materials. Hence, syngas production from catalytic CO_2 gasification of two representative feedstocks (polystyrene and pinewood) was investigated in this paper using a fixed-bed reactor at 900 °C. $Ni\text{-}Mg/Al_2O_3$ catalyst and a quasi in situ catalytic method were used in catalytic gasification. The characteristics of syngas evolution, syngas composition, and cold gas efficiency from catalytic and non-catalytic gasification were compared with elucidate the role of catalyst in catalytic CO_2-assisted gasification. The aim of this paper is to achieve effective conversion of diverse wastes such as plastic wastes and biowastes from catalytic CO_2-assisted gasification, which can support energy and environmental sustainability from the increased use of these waste materials.

2 Experimental

2.1 Feedstock Materials. Polystyrene and pinewood were used as representative plastic waste and biomass materials to evaluate their feasibility as feedstocks for energy recovery from catalytic CO_2-assisted gasification. Polystyrene pellets of 2 mm average size were obtained from Sigma-Aldrich. Pinewood pellets were provided by Drax Biomass with an average size of 8 mm. Both polystyrene and pinewood samples were dried at 105 °C for 12 h before use. Table 1 gives the lower heating values (LHVs), proximate analyses, and ultimate analyses of these feedstocks. The characterization studies of pinewood were performed using rapid calorimeter (5E-KCIII, Hunan, China), proximate analyzer (UV-02053-00, New Castle, DE, USA), and elemental analyzer (Vario EL cube, Langenselbold, Germany). The data on polystyrene were obtained from the literature [2,23].

2.2 Catalyst Preparation. $Ni\text{-}Mg/Al_2O_3$ catalyst was synthesized using a previously reported incipient wetness method [24,25]. A binary precursor solution containing Ni and Mg was first prepared from nickel nitrate hexahydrate ($Ni(NO_3)_2 \cdot 6H_2O$, Sigma-Aldrich) and magnesium nitrate hexahydrate ($Mg(NO_3)_2 \cdot 6H_2O$, Sigma-Aldrich). The concentrations of Ni and Mg in precursor solution were determined to obtain 10 wt% Ni loading and 4 wt% Mg loading on the calcined catalyst. $\gamma\text{-}Al_2O_3$ support (Alfa Aesar)

Table 1 LHV, proximate analyses, and ultimate analyses of polystyrene and pinewood

	LHV (MJ/kg)	Proximate analysis (wt%)[a]				Ultimate analysis (wt%)[b]				
		Moisture	Ash	Volatile	Fixed carbon	C	H	N	S	O[c]
Polystyrene	41.81	0	0	99.8	0.2	91.57	7.80	0.15	0.04	0.45
Pinewood	17.65	0.0	0.2	85.6	14.2	48.72	6.52	0.23	0.12	44.41

[a]Dry basis.
[b]Dry ash free basis.
[c]Calculated by difference.

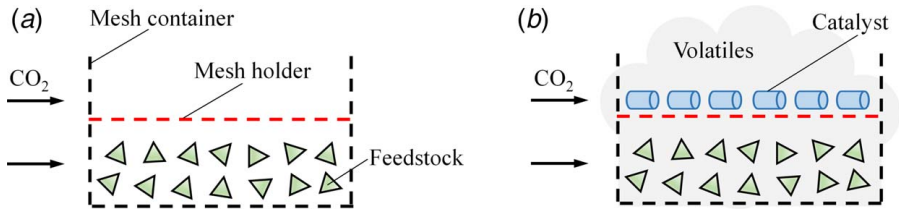

Fig. 1 Schematic diagram of (*a*) non-catalytic and (*b*) quasi-in situ catalytic methods

then was impregnated with the above precursor solution for 12 h. The obtained mixture was dried overnight at 105 °C and subsequently calcinated at 800 °C for 2 h. The synthesized catalyst was in the form of pellets with the characteristic size of 3 mm (diameter) × 4 mm (length).

2.3 Catalytic Method and Reactor Facility. Figure 1 shows the non-catalytic and quasi in situ catalytic methods used in this study. For non-catalytic tests, the feedstock was placed in a stainless-steel cylindrical mesh container and gasified in CO_2 atmosphere, see Fig. 1(*a*). The mesh container provided easy introduction of the sample in the test section and allowed efficient contact of feedstock with the incoming gasifying agent. For quasi in situ catalytic method, the feedstock was in the same configuration as that of non-catalytic method, but an extra catalyst layer supported on a mesh holder was placed immediately downstream of the feedstock layer for enhanced volatiles interaction with the catalyst, see Fig. 1(*b*). The distance between catalyst layer and feedstock layer was approximately 20 mm, which avoided the direct contact between catalyst and feedstock but allowed the catalytic conversion of gasified vapors on catalyst surface. Note that the quasi in situ catalytic method used in this paper is different from the in situ and ex situ catalytic methods reported in literature. In situ catalytic process is also called primary catalytic process, wherein feedstock and catalyst are typically evenly mixed in one reactor [26,27]. Ex situ catalytic process is also called secondary catalytic process, wherein feedstock and catalyst are placed in separated reactors and typically operated under different conditions [28]. Our previous study systematically compared different catalytic methods for polypropylene gasification and found that quasi in situ catalytic method showed superiority than in situ method in terms of H_2 generation and energy efficiency [19]. Quasi in situ catalytic method is also expected to reduce capital and operating costs compared with ex situ method since no downstream reactor is required [29]. Hence, quasi in situ catalytic method was used in this paper to investigate the role of catalyst in CO_2-assisted gasification.

Non-catalytic and catalytic gasification experiments were performed in a lab-scale fixed-bed reactor system, as shown in Fig. 2, which mainly consisted of two electrically heated furnaces (gas preheater and fixed-bed reactor), condensation unit, gas sampling unit and micro gas chromatograph (micro GC) measurement unit. Before each experiment, argon was used as the purge gas to ensure that the experimental test section was free of residual syngas from a previous run. CO_2 at flowrate of 1.58 l/min was used as the gasifying agent. N_2 at flowrate of 0.53 l/min was used as the tracer gas to calculate the mass flowrates of evolved syngas components based on GC measurements. The preheater and fixed-bed reactor temperatures were set at 900 °C, which provided a quasi-isothermal condition for catalytic gasification condition to support endothermic gasification reactions for syngas production. For each catalytic gasification experiment, 35 g of polystyrene or pinewood was loaded on a mesh support in the sample container as feedstock along with 11.67 g of catalyst (mass ratio of feedstock to catalyst 3:1). This feedstock to catalyst ratio was similar to those reported in catalytic steam gasification with Ni-based catalysts [18,21]. Reaction time was recorded as soon as the sample was introduced into isothermal section of the reactor.

The evolved product gases from fixed-bed reactor were split into two branches, with a small portion of gases passed through ice bath condensers to remove tar and moisture and the remaining gases vented out via an exhaust system. The tar and moisture free gas mixture was further pumped to gas sampling unit for GC measurements. An Agilent 3000A micro GC was calibrated to analyze the molar concentrations of CO_2, N_2, H_2, CO, CH_4, C_2H_6, C_2H_4, C_2H_2, and C_3H_8 with precision of ±0.1%. Our previous investigations in this fixed-bed reaction system showed that a considerable portion of product gases was evolved in the first 5 min [30–32]. However, the minimum sampling time of this GC was 2.67 min. To overcome GC sampling time limit, the product gases at 0.5, 1, 2, 3, and 4 min were stored in five stainless-steel gas sampling bottles for their later analysis. Thereafter, the evolved gases were continuously analyzed at GC sampling rate until 56 min from the start of gasification. Each experiment was repeated several times to ensure data reliability and the average values were reported. In this paper, the mixture of H_2, CO, CH_4, C_2H_6, C_2H_4, C_2H_2, and C_3H_8 was referred to as syngas.

3 Results and Discussion

3.1 Characteristic of Syngas Evolution. Figure 3 shows a comparison on the evolution and cumulative yields of (a) H_2, (b) CO, (c) CH_4, and (d) C_2-C_3 from non-catalytic and catalytic gasification of polystyrene (denoted as PS). C_2-C_3 presented here is the mixture of light hydrocarbons consisting of C_2H_2, C_2H_4, C_2H_6, and C_3H_8. As shown in Fig. 3(*a*), H_2 flowrate in non-catalytic gasification case increased steeply and peaked at 3 min after the PS sample was introduced to the fixed-bed reactor, followed by a sharp decrease from 3 to 12 min. Thereafter, H_2 release was not significant. The observed H_2 peak in non-catalytic case was mainly

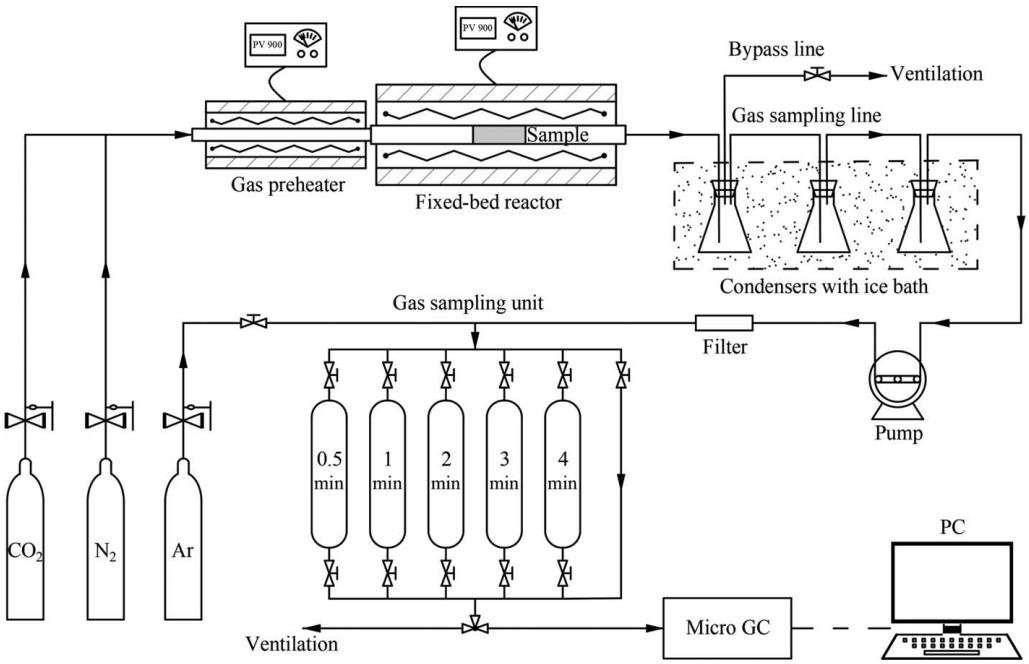

Fig. 2 Schematic diagram of the fixed-bed reactor system

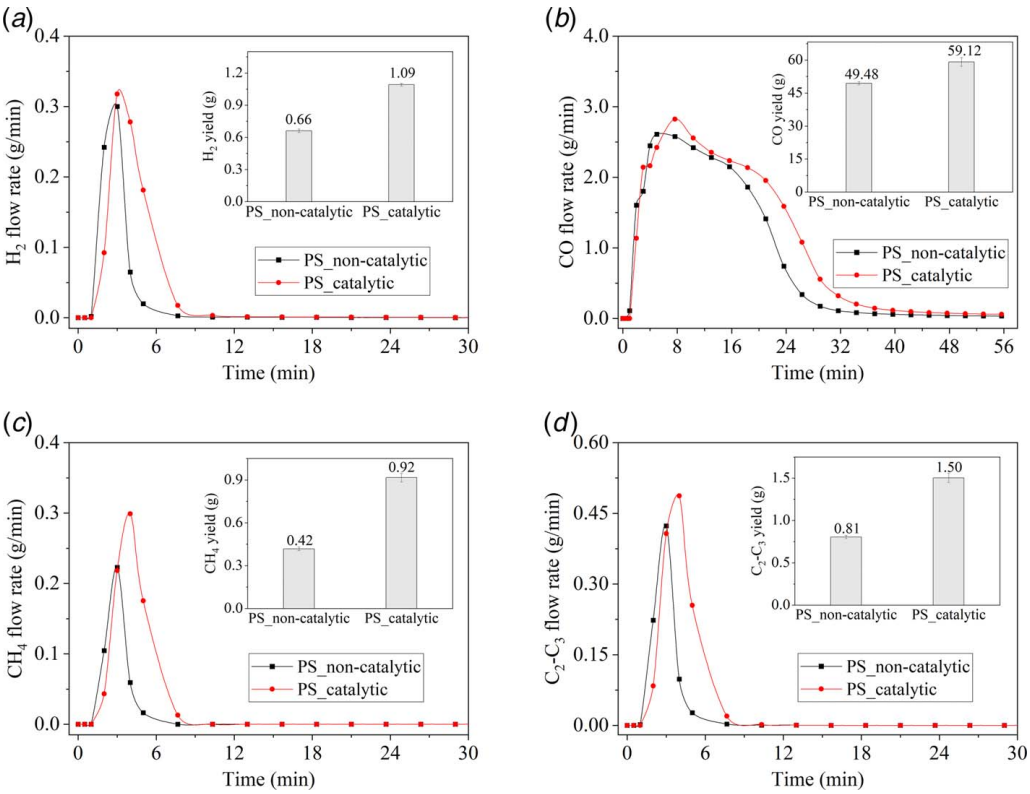

Fig. 3 Evolution and cumulative yields of (*a*) H_2, (*b*) CO, (c) CH_4, and (*d*) C_2-C_3 from non-catalytic and catalytic gasification of PS

ascribed to the flowing two pathways. On one hand, PS degradation proceeds via random scission mechanism [33]. The multi-step breakdown of PS backbone in parallel with intermolecular H-abstraction resulted in the generation of PS oligomers, such as monomeric, dimeric, and trimeric styrene. These PS oligomers underwent further cracking reactions driven by high thermal energy (900 °C) to produce H_2 and light hydrocarbons, see Eq. (1). On the other hand, due to the high aromatic content and good thermal stability, the cracking pathway of PS oligomers was incomplete, leading to the formation of a wide range of benzene derivatives such as toluene and ethylbenzene [34]. These benzene derivatives involved dry reformation reactions with CO_2 to generate H_2 and CO, see Eq. (2). A comparison of H_2 flowrate between non-catalytic and catalytic cases revealed significant enhancement of H_2

generation with the introduction of catalyst. The peak H_2 flowrate from catalytic gasification was higher than that from non-catalytic condition, and a noticeable promotion of H_2 flowrate was observed in catalytic gasification from 3 to 12 min. The cumulative H_2 yield was also enhanced by 63% from catalytic gasification as compared with the non-catalytic gasification. These results indicated that Ni-Mg/Al_2O_3 catalyst facilitated the primary cracking of PS oligomers to low molecular weight compounds and favored the CO_2 reforming of benzene derivatives from PS degradation, both contributing to enhanced H_2 formation. In addition, it is noteworthy that H_2 flowrate from catalytic gasification was lower than non-catalytic gasification at the beginning of the process from 0 to 2 min. This was mainly because the catalyst layer acted as a physical barrier that hindered the transport of evolved gases and vapors out of the sample holder, resulting in the slightly delayed evolution of H_2 and other gases components (see data from 0 to 2 min in Figs. 3(*b*)–3(*d*)). Furthermore, the catalyst used in this study was expected to undergo in situ reduction from the resulting gasification gases (H_2 and CO). This reduction process consumed a certain amount of H_2 during the initial gasification stage, which could be another contributor to the delayed H_2 evolution observed in catalytic gasification.

The evolution of CO flowrate under catalytic and non-catalytic gasification conditions is illustrated in Fig. 3(*b*). For non-catalytic PS gasification, CO flowrate peaked at 5 min, followed by a moderate decrease over a longtime duration until 56 min. The evolutionary behavior of CO presented here was different from that of H_2 shown in Fig. 3(*a*), wherein the evolution of H_2 was completed in a much shorter time duration and the evolved H_2 was negligible after 12 min. Note that the pyrolytic decomposition of PS does not yield any CO due to the absence of oxygenate. Hence, the evolved CO from 0 to 12 min in non-catalytic gasification case was attributed to dry reforming of PS oligomers and benzene derivatives from primary cracking. After 12 min, the breakdown of PS was still progressing with the release of vapors (tars) having higher aromaticity than styrene. Meanwhile, the benzene derivatives from primary cracking were recombined at high temperature via the secondary gas phase condensation reactions to form polycyclic aromatic hydrocarbons (PAHs). Lee et al. [34] reported that PAHs yield from PS pyrolysis accounted for approximately 60% in pyrolytic oil when the process temperature was over 800 °C. These aromatic vapors along with PAHs were reformed by the co-existing CO_2 at a relatively slow reaction rate, contributing to moderate CO evolution from 12 to 56 min. In addition, no solid residue (char) was found after the PS gasification, which is mainly ascribed to its extremely low fixed carbon content (0.2%). As for the catalytic gasification of PS, CO evolution profile was similar to that of non-catalytic gasification but with a noticeably higher evolution rate from 8 to 56 min. The cumulative CO yield in catalytic gasification was also elevated by some 20% than non-catalytic condition, revealing the effective enhancement of CO with the catalyst used. It is reported that Ni-based catalysts are one of the most effective transition metal catalysts for tar cracking and reforming [15]. In the present study, CO_2-assisted reforming of aromatic vapors and PAHs from PS degradation occurred when the resulting vapors passed through the catalyst layer. These CO_2 reforming reactions were characterized with slow reaction kinetics and can be catalytically expedited with the introduction of Ni-based catalyst [35,36], to promote CO formation. Additionally, the Ni-based catalyst enhanced the cracking of PAHs to mono aromatics and low molecular weight hydrocarbons which can be much more easily reformed with CO_2 to generate more CO. On the other hand, contact of pyrolytic vapors with catalyst led to the unwanted carbon deposition on catalyst surface. However, this problem can be alleviated with the addition of MgO in Ni-based catalyst [37]. MgO catalytically enhanced the Boudouard reaction of deposited carbon with CO_2 to produced CO (see Eq. (3)) [38], which could be another contributor to enhanced CO yield from catalytic gasification.

The evolutionary behaviors of CH_4 and C_2-C_3 were very similar under both catalytic and non-catalytic conditions, see Figs. 3(*c*) and 3(*d*). The peak flowrates of CH_4 and C_2-C_3 under non-catalytic condition were observed at 3 min; these peaks appeared slightly later with remarkably promoted peak values in catalyst gasification. The cumulative yields of CH_4 and C_2-C_3 in catalytic gasification were almost double than non-catalytic condition. The significant enhancements of CH_4 and C_2-C_3 from catalytic gasification were attributed to catalytic cracking of pyrolytic vapors from PS degradation [39], which favored the generation of H_2 and light hydrocarbons

$$(C_8H_8)_n \text{ (PS oligomers)} \rightarrow H_2 + C_xH_y + C_aH_b \quad (1)$$

$$C_nH_m \text{ (Benzene derivatives)} + nCO_2 \rightarrow \frac{m}{2}H_2 + 2nCO \quad (2)$$

$$C(s) + CO_2 \leftrightarrow 2CO \quad (3)$$

Figure 4 shows a comparison on the evolutionary behavior and cumulative yields of (a) H_2, (b) CO, (c) CH_4, and (d) C_2-C_3 from non-catalytic and catalytic gasification of pinewood (denoted as PW). Catalytic gasification resulted in a drastic enhancement of H_2 formation, Fig. 4(*a*). The peak H_2 flowrate from non-catalytic gasification was 0.08 g/min, while this value increased to 0.20 g/min under catalytic condition. H_2 flowrate from catalytic gasification were also much higher than non-catalytic condition from 3 to 16 min. The enhancement of H_2 formation in catalytic PW gasification can be ascribed to the catalytic conversion of pyrolytic vapors, which included the enhanced cracking of pyrolytic vapors (tars) to H_2 and enhanced CO_2 dry reforming of resulting vapors to H_2 and CO. These pathways for H_2 yield enhancement were similar to those possible in PS catalytic gasification. However, a more pronounced enhancement was observed in catalytic gasification of PW than that of PS. The cumulative H_2 yield was promoted by 150% from catalytic PW gasification (see Fig. 4(*a*)), as compared with the 63% enhancement of H_2 obtained from catalytic PS gasification (see Fig. 3(*a*)). A relatively greater improvement in H_2 yield from catalytic gasification of PW could be attributed to its relatively low aromaticity compared with PS. More specifically, PW is a representative lignocellulosic biomass that consists of cellulose, hemicellulose, and lignin [40]. Even though the hydrogen content of PW and PS are very close (see Table 1), considerable amounts of H in PW exist in the glucose units of cellulose and hemicellulose, along a small portion of H exists in the aromatic matrix of lignin [41]. While in the case of PS, a large portion of H exists in benzene ring on account of its high aromatic content. During the catalytic gasification, PW decomposition occurred with the release of glucose, levoglucosan, and other low molecular weight oxygenates [42]. These primary products from PW decomposition can be much more easily catalytically cracked than benzene derivatives and PAHs from PS degradation, thereby contributing to a greater enhancement of H_2 yield from catalytic PW gasification.

Evolutionary behavior and cumulative yield of CO from non-catalytic and catalytic PW gasification are presented in Fig. 4(*b*). Under non-catalytic gasification condition, CO flowrate exhibited an evolution peak at 3 min, followed by a plateau behavior for long duration from reaction time of 16–56 min. The observed CO evolution peak can be ascribed to pyrolytic breakdown of PW at high temperature generating low molecular weight oxygenates, which underwent further decarbonylation to release CO [43]. In addition, the CO_2 dry reforming of pyrolytic vapors from primary cracking also contributed to CO formation during this period. After the reaction time of 16 min, CO flowrate showed almost a plateau behavior. Our previous study on PW pyrolysis at 900 °C revealed that the pyrolytic reactions of PW were completed in 16 min and the CO evolution after that time was negligible. Considerable amounts of char residue (around 19 wt%) were also obtained from PW pyrolysis [32]. The observed plateau behavior of CO evolution shown in Fig. 4(*b*) was mainly attributed to Boudouard

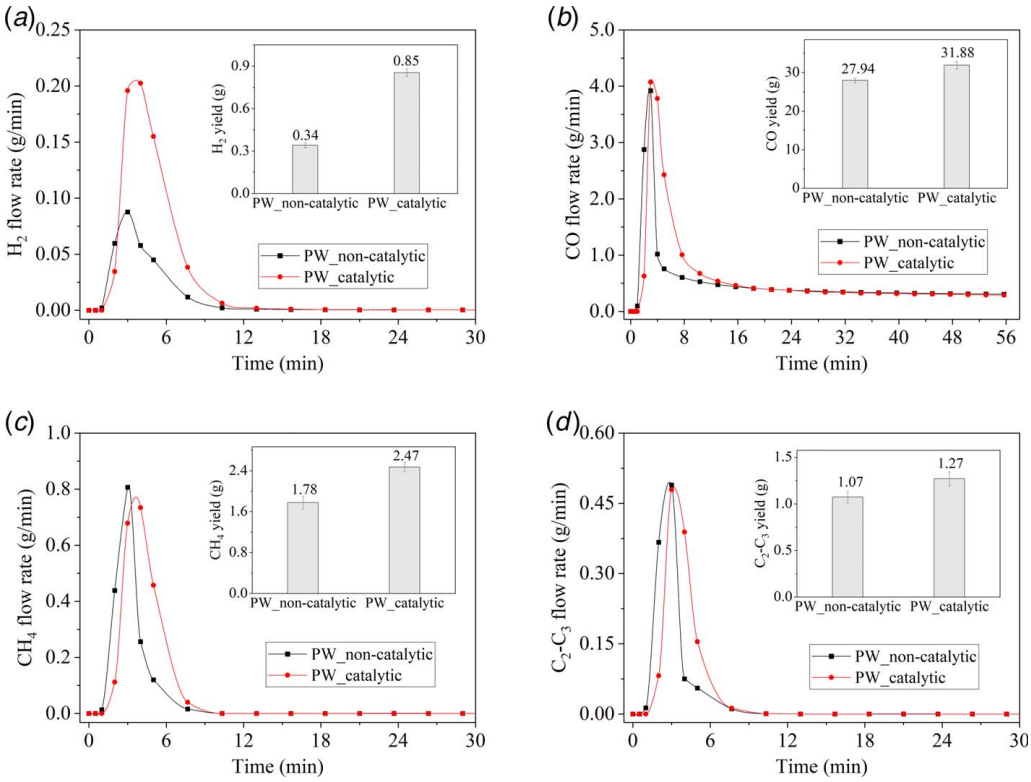

Fig. 4 Evolution and cumulative yields of (*a*) H_2, (*b*) CO, (c) CH_4, and (*d*) C_2-C_3 from non-catalytic and catalytic gasification of PW

reaction in which PW char gasified with CO_2 at slow reaction rate to generate CO. Furthermore, the evolutionary behavior of CO shown in Fig. 4(*b*) revealed that catalytic gasification produced higher CO flowrate than non-catalytic condition from 3 to 16 min. The enhanced CO yield during this period can be explained by the promoted CO_2 reforming of pyrolytic vapors with Ni-based catalyst. While after the reaction time of 16 min, CO flowrates from catalytic and non-catalytic gasification coincided with each other to reveal similar plateau behavior of CO evolution in both gasification cases. Note that in catalytic PW gasification, catalyst was placed downstream of PW (see Fig. 1(*b*)) to ensure the resulting pyrolytic vapors in good contact with the catalytic layer. This configuration on the other hand excluded the contact of PW char with catalyst, and accordingly the char gasification via Boudouard reaction was not impacted with the introduction of catalyst, as seen from the comparable CO flowrates from non-catalytic and catalytic gasification after 16 min. Figure 4(*b*) also shows the cumulative yield of CO was promoted by 14% with catalytic gasification, mainly resulting from the facilitated CO_2 reforming of pyrolytic vapors.

Evolution of CH_4 flowrate shown in Fig. 4(*c*) reveals a remarkable enhancement of CH_4 yield from catalytic gasification as compared with non-catalytic condition. Even though the peak CH_4 flowrate from catalytic gasification was comparable to non-catalytic gasification, catalytic gasification resulted in a higher CH_4 flowrate from 4 to 12 min due to enhanced primary cracking reactions in the presence of catalyst. Figure 4(*d*) shows that similar enhancement of C_2-C_3 yield can be obtained with catalytic gasification, further confirming that catalyst used in this study enhanced the cracking of pyrolytic vapors from PW decomposition. The results on cumulative yields of CH_4 and C_2-C_3 from PW gasification showed enhancement by 39% and 16%, respectively, with the introduction of catalyst.

Figure 5 shows the evolution and cumulative yield of total syngas from gasification of (a) PS and (b) PW under non-catalytic and

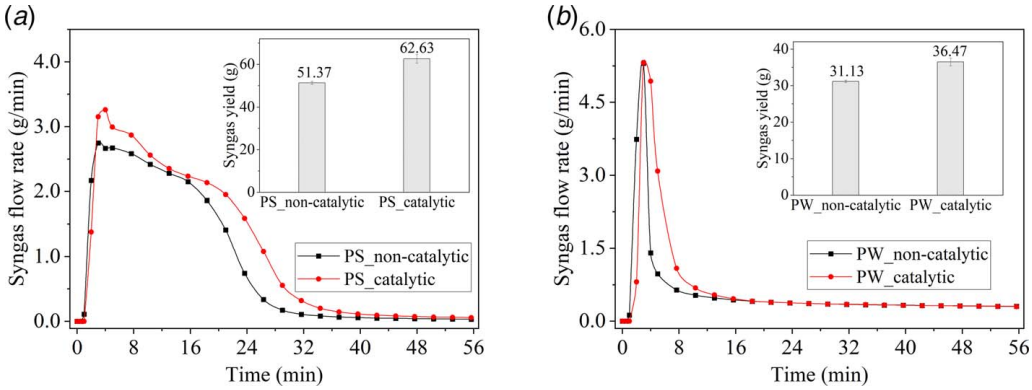

Fig. 5 Evolution and cumulative yields of syngas from gasification of (*a*) PS and (*b*) PW under non-catalytic and catalytic conditions

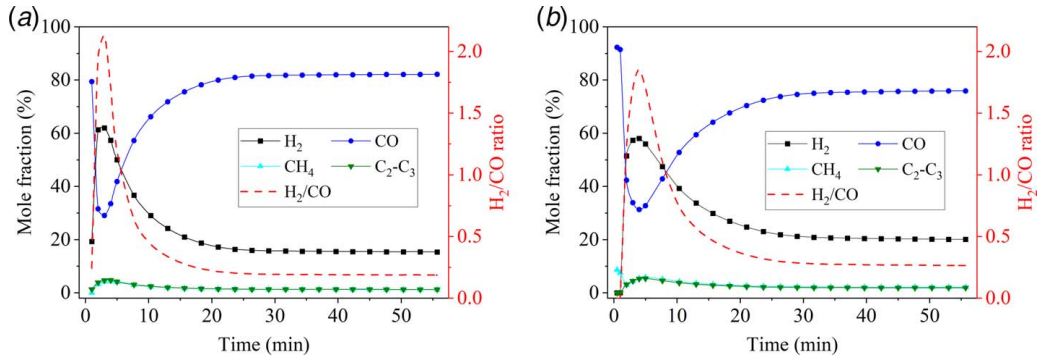

Fig. 6 Mole fractions of gas components in accumulated syngas gas yield from (*a*) non-catalytic and (*b*) catalytic gasification of PS

catalytic conditions. Syngas reported here is the mixture of gas components of H_2, CO, CH_4, and C_2-C_3. A noticeable enhancement of syngas flowrate was observed in catalytic gasification, see Fig. 5. In addition, the evolutionary behavior of syngas was similar to that of CO shown in Figs. 3(*b*) and 4(*b*), mainly because CO was the dominant component in syngas from CO_2-assisted gasification. The cumulative syngas yields from catalytic gasification of PS and PW were enhanced by 22% and 17%, respectively, as compared with non-catalytic gasification, indicating that the Ni-Mg/Al_2O_3 catalyst was favorable for CO_2 gasification for the diverse feedstocks (waste plastics and biomass) in terms of promoted syngas production and reduced tar formation.

3.2 Characteristic of Syngas Composition. Figure 6 shows mole fractions of gas components in the accumulated syngas gas yield from (a) non-catalytic and (b) catalytic gasification of PS. The results can be helpful in determining the extent of reaction time at which gasification can be stopped to obtain syngas of desired quality based on its composition [44]. As shown in Fig. 6, the mole fractions of H_2, CH_4, and C_2-C_3 exhibited a rapid increase in the initial gasification stage and then gradually decreased as the reaction time prolonged under both non-catalytic and catalytic conditions, while an opposite trend was observed for CO mole fraction. The steep increase in mole fractions of H_2, CH_4, and C_2-C_3 was attributed to intense primary cracking of PS at high temperatures with considerable release of these gases in the initial gasification stage. From reaction time of 12–35 min, the release of H_2 and light hydrocarbons was not significant, but CO continued to evolve from CO_2 dry reforming of benzene derivatives and PAHs derived from the further breakdown of PS (see Fig. 3). This resulted in the observed moderate increase of CO mole fraction during this period. After the reaction time of 35 min, mole fractions of all gas components remained almost unchanged. Moreover, the introduction of catalyst in PS gasification resulted in a promotion in mole fractions of H_2, CH_4, and C_2-C_3 at a certain reaction time, along with declined CO mole fraction even though the net CO yield was enhanced from catalytic gasification (see Fig. 3(*a*)). After reaction time of 35 min, catalytic gasification brought a noticeable increase in H_2/CO ratio from 0.19 to 0.26, which is an important index that dictates the use of syngas for direct thermal energy production or synthetization of value-added chemicals [45].

Figure 7 shows mole fractions of gas components in accumulated syngas gas yield from (a) non-catalytic and (b) catalytic gasification of PW. As compared with PS gasification, the moles fractions of syngas components from PW gasification underwent a relatively moderate change with reaction time. Specially, CO mole fraction slightly decreased and then continuously increased until the end of gasification under both non-catalytic and catalytic conditions. The slight decrease in CO mole fraction in the initial gasification stage was attributed to the intense release of other gas components (H_2, CH, and C_2-C_3) from the pyrolytic breakdown of PW. Thereafter, the decomposition of PW was completed with a considerable amount of char formed. The resulting char was slowly gasified with CO_2 via Boudouard reaction contributing to the continuously increased CO mole fraction until the end of gasification. In addition, PW gasification under catalytic condition caused a remarkable increase in H_2/CO ratio from 0.17 to 0.37 at 56 min, which was similar to that observed in catalytic PS gasification.

Figure 8 further shows (a) mole fractions and (b) energy fractions of gas components in the accumulated syngas yield over 56 min from gasification of PS and PW under non-catalytic and catalytic conditions. As shown in Fig. 8(*a*), CO shared the highest volume fraction in syngas under all conditions. This result was expected since CO_2-assisted gasification typically produced CO-rich syngas from dry reforming and Boudouard reactions [46]. For PS gasification, the introduction of catalyst resulted in elevated H_2 (from 15.4% to 20.1%), CH_4 (from 1.2% to 2.1%), and C_2-C_3 mole fractions (from 1.3% to 1.9%), and accordingly decreased CO mole fraction

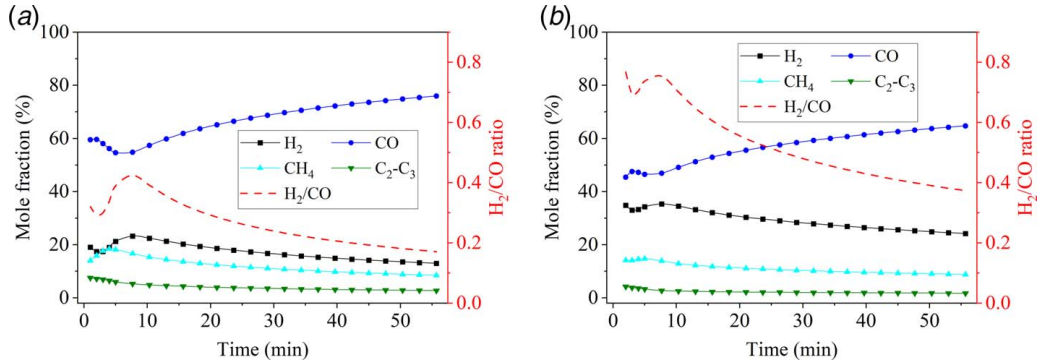

Fig. 7 Mole fractions of gas components in accumulated syngas gas yield from (*a*) non-catalytic and (*b*) catalytic gasification of PW

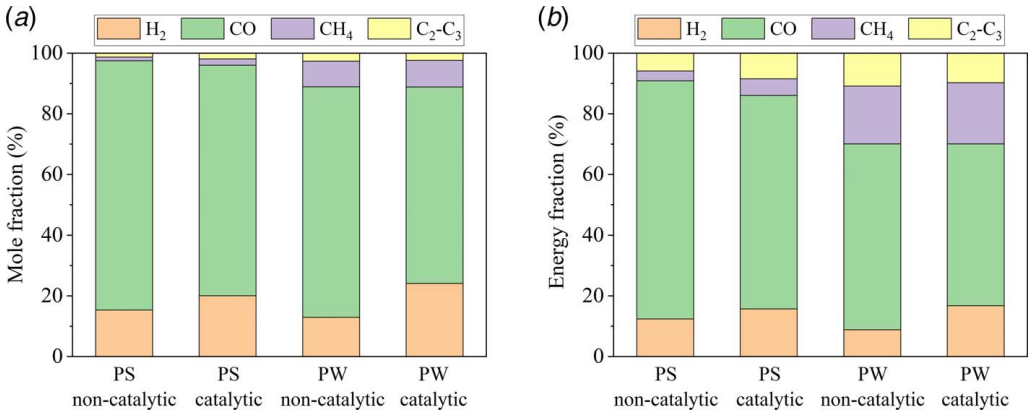

Fig. 8 (*a*) Mole fractions and (*b*) energy fractions of gas components in accumulated syngas yield over 56 min from gasification of PS and PW under non-catalytic and catalytic conditions

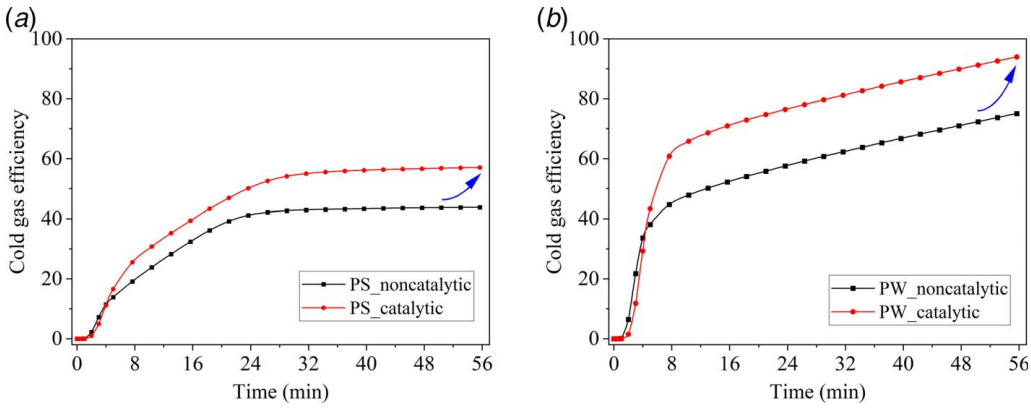

Fig. 9 Comparison of cold gas efficiency from gasification of (*a*) PS and (*b*) PW under non-catalytic and catalytic conditions

from 82.1% to 75.9%. While for PW gasification, catalyst brought a more pronounced enhancement in H_2 mole fraction from 12.9% to 24.2%, but the CO mole fraction remarkably declined from 75.9% to 64.7%. The increase in H_2 mole fraction along with decreased CO mole fraction revealed enhanced syngas quality, which not only supports the clean combustion of syngas for direct energy production, but also promotes the versatility in its further utilization to synthesize value-added chemicals. Figure 8(*b*) shows the energy composition of accumulated syngas. Energy composition presented here was calculated based on mass fractions of syngas components along with their LHVs, which reveals the contribution of each gas component to the overall syngas energy. As shown in Fig. 8(*b*), CO was the primary contributor to syngas energy, which accounted for 78.5% and 61.2% in gasification of PS and PW, respectively. The introduction of catalyst caused reduction in CO contribution but increased H_2 contribution to syngas energy. Moreover, due to the changed syngas composition under catalytic condition, the average LHV of syngas was increased from 12.47 to 13.62 MJ/kg in catalytic PS gasification, and from 14.90 to 16.69 MJ/kg in catalytic PW gasification.

3.3 Characteristic of Cold Gas Efficiency. Cold gas efficiency reported here was defined as the ratio of calorific content of evolved syngas (E_{syngas}) to calorific content of initial feedstock ($E_{feedstock}$), see Eq. (4)

$$\text{Coldgas efficiency} = \frac{E_{syngas}}{E_{feedstock}} \times 100\% \tag{4}$$

Figure 9 shows the comparison of cold gas efficiency from gasification of (a) PS and (b) PW under non-catalytic and catalytic conditions. The gasification of PS and PW yielded different behaviors in cold gas efficiency, see Fig. 9. For PS gasification, cold gas efficiency increased at a moderate rate from 0 to 32 min followed by a plateau behavior. However, in the case of PW gasification, cold gas efficiency increased steeply in the initial gasification stage (0–12 min) followed by a steady continuous increase until the end of gasification. The differences in evolution of cold gas efficiencies between PS and PW could be attributed to the different characteristics of syngas evolution. Specifically, PS was relatively stable and decomposed at a lower rate than PW due to the higher aromatic content, which resulted in moderate syngas evolution over a long-time duration (see from 0 to 32 min in Fig. 4(*a*)). After 32 min, PS decomposition almost completed and the evolved syngas from PS gasification was not significant. In contrast, PW decomposition proceeded rapidly with the intense syngas evolving from 0 to 12 min (see Fig. 4(*b*)). After that, a considerable amount of char formed and was gasified with CO_2 at low reaction rate to generate CO, which was responsible for the continuous increase in cold gas efficiency from 12 to 56 min. Furthermore, since catalyst significantly promoted syngas formation by facilitated cracking and dry reforming reactions, the cold gas efficiency for PS gasification at 56 min was enhanced from 44% to 57%. An even more pronounced increase in the cold gas efficiency from 75% to 94% was obtained from catalytic PW gasification. These results indicate that catalytic CO_2-assisted gasification could be a promising pathway for efficient energy production from wastes plastics and biomass.

4 Conclusions

This paper reported the characteristics of syngas from catalytic gasification of diverse wastes such as polystyrene and pinewood

in CO_2 atmosphere using a fixed-bed reactor at 900 °C temperature. Based on the experimental results, the following conclusions can be drawn:

(1) Syngas yields from catalytic CO_2 gasification of polystyrene and pinewood were enhanced by 22% and 17%, respectively, as compared with non-catalytic conditions. This increase is mainly attributed to the improved cracking and CO_2 reforming reactions.
(2) Addition of Ni-Mg/Al_2O_3 catalyst to polystyrene gasification led to enhancement of 63% H_2, 20% CO, 119% CH_4, and 85% C_2–C_3 yields. In comparison, Ni-Mg/Al_2O_3 catalyst resulted in increase of 150% H_2, 14% CO, 39% CH_4, and 16% C_2–C_3 yields from pinewood gasification.
(3) A comparison of syngas composition between non-catalytic and catalytic conditions revealed improved syngas quality in catalytic gasification with increased H_2 mole fraction along with decreased CO mole fraction.
(4) Cold gas efficiency was significantly improved in the presence of catalyst, which increased from 44% to 57% in catalytic polystyrene gasification and from 75% to 94% in catalytic pinewood gasification.

Acknowledgment

This research was supported by Office of Naval Research and their support is gratefully acknowledged. The support provided to the authors (Xuan Liu, Zhiwei Wang, and Jinhu Li) from China Scholarship Council (CSC201906280344) is gratefully acknowledged. K. G. Burra was supported by Ann G. Wylie Fellowship and this is gratefully acknowledged.

Conflict of Interest

There are no conflicts of interest.

Data Availability Statement

The datasets generated and supporting the findings of this paper are obtainable from the corresponding author upon reasonable request. The authors attest that all data for this study are included in the paper. Data provided by a third party listed in Acknowledgment. No data, models, or code were generated or used for this paper.

References

[1] EPA, 2020, *Advancing Sustainable Materials Management: 2018 Fact Sheet Assessing Trends in Material Generation and Management in the United States*, United States Environmental Protection Agency, Research Triangle Park, Durham, NC.
[2] Park, K.-B., Jeong, Y.-S., Guzelciftci, B., and Kim, J.-S., 2020, "Two-Stage Pyrolysis of Polystyrene: Pyrolysis Oil as a Source of Fuels or Benzene, Toluene, Ethylbenzene, and Xylenes," Appl. Energy, **259**, p. 114240.
[3] Burra, K. G., and Gupta, A. K., 2018, "Synergistic Effects in Steam Gasification of Combined Biomass and Plastic Waste Mixtures," Appl. Energy, **211**, pp. 230–236.
[4] Rahimi, A., and García, J. M., 2017, "Chemical Recycling of Waste Plastics for New Materials Production," Nat. Rev. Chem., **1**(6), p. 0046.
[5] Yang, S.-S., Brandon, A. M., Andrew Flanagan, J. C., Yang, J., Ning, D., Cai, S.-Y., Fan, H.-Q., Wang, Z.-Y., Ren, J., Benbow, E., Ren, N.-Q., Waymouth, R. M., Zhou, J., Criddle, C. S., and Wu, W.-M., 2018, "Biodegradation of Polystyrene Wastes in Yellow Mealworms (Larvae of Tenebrio Molitor Linnaeus): Factors Affecting Biodegradation Rates and the Ability of Polystyrene-Fed Larvae to Complete Their Life Cycle," Chemosphere, **191**, pp. 979–989.
[6] Moore, C. J., 2008, "Synthetic Polymers in the Marine Environment: A Rapidly Increasing, Long-Term Threat," Environ. Res., **108**(2), pp. 131–139.
[7] Chae, Y., and An, Y.-J., 2017, "Effects of Micro- and Nanoplastics on Aquatic Ecosystems: Current Research Trends and Perspectives," Mar. Pollut. Bull., **124**(2), pp. 624–632.
[8] Lehner, R., Weder, C., Petri-Fink, A., and Rothen-Rutishauser, B., 2019, "Emergence of Nanoplastic in the Environment and Possible Impact on Human Health," Environ. Sci. Technol., **53**(4), pp. 1748–1765.
[9] Anuar Sharuddin, S. D., Abnisa, F., Wan Daud, W. M. A., and Aroua, M. K., 2017, "Energy Recovery From Pyrolysis of Plastic Waste: Study on Non-Recycled Plastics (NRP) Data as the Real Measure of Plastic Waste," Energy Convers. Manage., **148**, pp. 925–934.
[10] Sheldon, R. A., 2014, "Green and Sustainable Manufacture of Chemicals From Biomass: State of the Art," Green Chem., **16**(3), pp. 950–963.
[11] Liu, X., Ca, W., Zhu, T., Lv, Q., Li, Y., and Che, D., 2019, "Simultaneous Removal of NO_x and SO_2 From Coal-Fired Flue Gas Based on the Catalytic Decomposition of H_2O_2 Over $Fe_2(MoO_4)_3$," Chem. Eng. J., **371**, pp. 486–499.
[12] Al-Zareer, M., Dincer, I., and Rosen, M. A., 2018, "Influence of Selected Gasification Parameters on Syngas Composition From Biomass Gasification," ASME J. Energy Resour. Technol., **140**(4), p. 041803.
[13] Herdem, M. S., Lorena, G., and Wen, J. Z., 2019, "Simulation and Performance Investigation of a Biomass Gasification System for Combined Power and Heat Generation," ASME J. Energy Resour. Technol., **141**(11), p. 112002.
[14] Basha, M. H., Sulaiman, S. A., and Uemura, Y., 2020, "Co-Gasification of Palm Kernel Shell and Polystyrene Plastic: Effect of Different Operating Conditions," J. Energy Inst., **93**(3), pp. 1045–1052.
[15] Chan, F. L., and Tanksale, A., 2014, "Review of Recent Developments in Ni-Based Catalysts for Biomass Gasification," Renewable Sustainable Energy Rev., **38**, pp. 428–438.
[16] Lopez, G., Artetxe, M., Amutio, M., Alvarez, J., Bilbao, J., and Olazar, M., 2018, "Recent Advances in the Gasification of Waste Plastics. A Critical Overview," Renewable Sustainable Energy Rev., **82**(Part 1), pp. 576–596.
[17] Inayat, M., Sulaiman, S. A., Kurnia, J. C., and Shahbaz, M., 2019, "Effect of Various Blended Fuels on Syngas Quality and Performance in Catalytic Co-Gasification: A Review," Renewable Sustainable Energy Rev., **105**, pp. 252–267.
[18] Xu, D., Xiong, Y., Ye, J., Su, Y., Dong, Q., and Zhang, S., 2020, "Performances of Syngas Production and Deposited Coke Regulation During Co-Gasification of Biomass and Plastic Wastes Over Ni/γ-Al_2O_3 Catalyst: Role of Biomass to Plastic Ratio in Feedstock," Chem. Eng. J., **392**, p. 123728.
[19] Wang, Z., Liu, X., Burra, K. G., Li, J., Zhang, M., Lei, T., and Gupta, A. K., 2021, "Towards Enhanced Catalytic Reactivity in CO_2-Assisted Gasification of Polypropylene," Fuel, **284**, p. 119076. . Paper is January 15, 2021.
[20] Ruoppolo, G., Ammendola, P., Chirone, R., and Miccio, F., 2012, "H_2-Rich Syngas Production by Fluidized Bed Gasification of Biomass and Plastic Fuel," Waste Manag., **32**(4), pp. 724–732.
[21] Alvarez, J., Kumagai, S., Wu, C., Yoshioka, T., Bilbao, J., Olazar, M., and Williams, P. T., 2014, "Hydrogen Production From Biomass and Plastic Mixtures by Pyrolysis-Gasification," Int. J. Hydrogen Energy, **39**(21), pp. 10883–10891.
[22] Kim, J.-W., Mun, T.-Y., Kim, J.-O., and Kim, J.-S., 2011, "Air Gasification of Mixed Plastic Wastes Using a Two-Stage Gasifier for the Production of Producer Gas With Low Tar and a High Caloric Value," Fuel, **90**(6), pp. 2266–2272.
[23] Ahmad, N., Ahmad, N., Maafa, I. M., Ahmed, U., Akhter, P., Shehzad, N., Amjad, U.-e-S., and Hussain, M., 2020, "Thermal Conversion of Polystyrene Plastic Waste to Liquid Fuel via Ethanolysis," Fuel, **279**, p. 118498.
[24] Efika, C. E., Wu, C., and Williams, P. T., 2012, "Syngas Production From Pyrolysis–Catalytic Steam Reforming of Waste Biomass in a Continuous Screw Kiln Reactor," J. Anal. Appl. Pyrolysis., **95**, pp. 87–94.
[25] Wu, C., and Williams, P. T., 2009, "Hydrogen Production From the Pyrolysis −Gasification of Polypropylene: Influence of Steam Flow Rate, Carrier Gas Flow Rate and Gasification Temperature," Energy Fuels, **23**(10), pp. 5055–5061.
[26] Chen, G., Liu, F., Guo, X., Zhang, Y., Yan, B., Cheng, Z., Xiao, L., Ma, W., and Hou, L., 2018, "Co-gasification of Acid Hydrolysis Residues and Sewage Sludge in a Downdraft Fixed Gasifier With CaO as an In-Bed Additive," Energy Fuels, **32**(5), pp. 5893–5900.
[27] Inayat, M., Sulaiman, S. A., and Kurnia, J. C., 2019, "Catalytic Co-Gasification of Coconut Shells and Oil Palm Fronds Blends in the Presence of Cement, Dolomite, and Limestone: Parametric Optimization via Box Behnken Design," J. Energy Inst., **92**(4), pp. 871–882.
[28] Galadima, A., and Muraza, O., 2015, "In Situ Fast Pyrolysis of Biomass With Zeolite Catalysts for Bioaromatics/Gasoline Production: A Review," Energy Convers. Manage., **105**, pp. 338–354.
[29] Colby, J. L., Dauenhauer, P. J., and Schmidt, L. D., 2008, "Millisecond Autothermal Steam Reforming of Cellulose for Synthetic Biofuels by Reactive Flash Volatilization," Green Chem., **10**(7), pp. 773–783.
[30] Wang, Z., Li, J., Burra, K. G., Liu, X., Li, X., Zhang, M., Lei, T., and Gupta, A. K., 2021, "Synergetic Effect on CO_2-Assisted Co-Gasification of Biomass and Plastics," ASME J. Energy Resour. Technol., **143**(3), p. 031901.
[31] Li, J., Burra, K. G., Wang, Z., Liu, X., Kerdsuwan, S., and Gupta, A. K., 2021, "Energy Recovery From Composite Acetate Polymer-Biomass Wastes via Pyrolysis and CO_2-Assisted Gasification," ASME J. Energy Resour. Technol., **143**(4), p. 042305.
[32] Liu, X., Burra, K. G., Wang, Z., Li, J., Che, D., and Gupta, A. K., 2020, "On Deconvolution for Understanding Synergistic Effects in Co-Pyrolysis of Pinewood and Polypropylene," Appl. Energy, **279**, p. 115811.
[33] Horton, S. R., Woeckener, J., Mohr, R., Zhang, Y., Petrocelli, F., and Klein, M. T., 2016, "Molecular-Level Kinetic Modeling of the Gasification of Common Plastics," Energy Fuels, **30**(3), pp. 1662–1674.
[34] Lee, T., Jung, S., Park, Y.-K., Kim, T., Wang, H., Moon, D. H., and Kwon, E. E., 2020, "Catalytic Pyrolysis of Polystyrene Over Steel Slag Under CO_2 Environment," J. Hazard. Mater., **395**, p. 122576.
[35] Yan, Y., Yan, H., Li, L., Zhang, L., and Yang, Z., 2018, "Thermodynamic Analysis on Reaction Characteristics of the Coupling Steam, CO_2 and O_2 Reforming of Methane," ASME J. Energy Resour. Technol., **140**(10), p. 102203.

[36] Garcia, L., Salvador, M. L., Arauzo, J., and Bilbao, R., 2001, "CO_2 as a Gasifying Agent for Gas Production From Pine Sawdust at Low Temperatures Using a Ni/Al Coprecipitated Catalyst," Fuel Process. Technol., **69**(2), pp. 157–174.
[37] Leung, D. Y. C., Yin, X. L., and Wu, C. Z., 2004, "A Review on the Development and Commercialization of Biomass Gasification Technologies in China," Renewable Sustainable Energy Rev., **8**(6), pp. 565–580.
[38] Lahijani, P., Zainal, Z. A., Mohammadi, M., and Mohamed, A. R., 2015, "Conversion of the Greenhouse Gas CO_2 to the Fuel Gas CO via the Boudouard Reaction: A Review," Renewable Sustainable Energy Rev., **41**, pp. 615–632.
[39] Noichi, H., Uddin, A., and Sasaoka, E., 2010, "Steam Reforming of Naphthalene as Model Biomass Tar Over Iron–Aluminum and Iron–Zirconium Oxide Catalyst Catalysts," Fuel Process. Technol., **91**(11), pp. 1609–1616.
[40] Wang, S., Dai, G., Yang, H., and Luo, Z., 2017, "Lignocellulosic Biomass Pyrolysis Mechanism: A State-of-the-Art Review," Progr. Energy Combust. Sci., **62**, pp. 33–86.
[41] Liu, Q., Wang, S., Zheng, Y., Luo, Z., and Cen, K., 2008, "Mechanism Study of Wood Lignin Pyrolysis by Using TG–FTIR Analysis," J. Anal. Appl. Pyrolysis., **82**(1), pp. 170–177.
[42] Persson, H., and Yang, W., 2019, "Catalytic Pyrolysis of Demineralized Lignocellulosic Biomass," Fuel, **252**, pp. 200–209.
[43] Horton, S. R., Mohr, R. J., Zhang, Y., Petrocelli, F. P., and Klein, M. T., 2016, "Molecular-Level Kinetic Modeling of Biomass Gasification," Energy Fuels, **30**(3), pp. 1647–1661.
[44] Wang, Z., Burra, K. G., Zhang, M., Li, X., He, X., Lei, T., and Gupta, A. K., 2020, "Syngas Evolution and Energy Efficiency in CO_2-Assisted Gasification of Pine Bark," Appl. Energy, **269**, p. 114996.
[45] Cao, Y., Gao, Z., Jin, J., Zhou, H., Cohron, M., Zhao, H., Liu, H., and Pan, W., 2008, "Synthesis Gas Production With an Adjustable H_2/CO Ratio Through the Coal Gasification Process: Effects of Coal Ranks and Methane Addition," Energy Fuels, **22**(3), pp. 1720–1730.
[46] Matas Güell, B., Sandquist, J., and Sørum, L., 2012, "Gasification of Biomass to Second Generation Biofuels: A Review," ASME J. Energy Resour. Technol., **135**(1), p. 014001.